Chapter 3

Overview of PatLoc Imaging and Presentation of Initial Hardware Designs

THE acronym *PatLoc = Parallel Imaging Technique using Localized Gradients* covers the two main aspects of this novel imaging modality: In PatLoc, signals are encoded with a *new type of gradient system* and received with several RF-receiver coils *in parallel*. The acronym implies that the PatLoc project included significant efforts in hardware development. This is certainly an important aspect, but the primary relevance of PatLoc for MRI is a conceptually new approach to MRI signal encoding with the ultimate goal of providing new means to generate innovative applications for medical diagnosis. The concept of PatLoc and arising applications are illustrated in this section and two hardware implementations are presented, which were developed during the course of the PatLoc project.

This chapter is special in that the presented material is based on work that has been performed by several members of the PatLoc team. The emphasis is placed on topics with significant own contributions, documented through (co-)authorship in various publications, among the most relevant to this chapter are [[61, 156, 42, 207, 63, 199, 24]].

3.1 The Concept

Since the advent of MRI, gradients were built with preferably linear field geometries. The PatLoc approach breaks with this tradition by intentionally introducing *nonlinear and non-bijective spatial encoding magnetic fields* (NB-SEMs). This conceptual extension of the signal encoding process has dramatic consequences for MRI signal localization.

Interestingly, some of the most fundamental effects of non-bijective encoding can be understood with a simple 1D example. Consider Fig. 3.1. In this example, a magnetic encoding field with quadratic geometry $\psi(x) \propto x^2$

G. Schultz, *Magnetic Resonance Imaging with Nonlinear Gradient Fields*,
DOI 10.1007/978-3-658-01134-5_3, © Springer Fachmedien Wiesbaden 2013

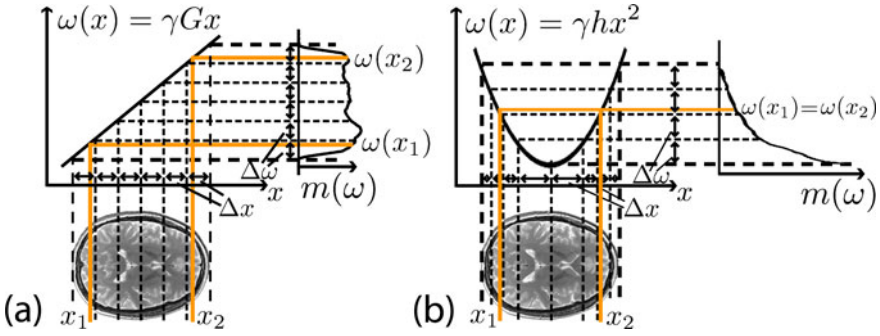

Figure 3.1: Concept of PatLoc imaging. (a) Conventional gradient encoding (cf. Fig. 1.7). (b) PatLoc encoding with a quadratic field. It is shown how the frequency content of the MR signal is linked to the location of origin via the magnetic encoding fields. The notation conforms to the main text. The comparison reveals differences to conventional encoding: First, as indicated by the thin dashed lines, the nonlinearity of the encoding field has the consequence that the voxel size (Δx) and therefore also image resolution is not homogeneous. Second, as indicated by the orange lines, the non-bijectiveness of the encoding fields has the consequence that different locations of the image are encoded with the same frequency. One advantage is a doubling of image resolution (on average). However, it is not possible to unambiguously determine the source location of the signal if encoding is solely done with such a non-bijective field.

instead of the traditional linear geometry $\psi_{grad}(x) \propto x$ is considered. The quadratic function differs in two ways from the linear function:

First, it is nonlinear. This nonlinearity has the consequence that image resolution is spatially dependent in PatLoc. The resolution increases with increasing steepness of the SEM. More subtle is the observation that the SNR is expected to decrease, where the encoding fields are steeper. This can be concluded from the low signal energy resulting from those steep regions as indicated by the $m(\omega)$-plots in Fig. 3.1. This behavior is in agreement with conventional Fourier imaging (cf. Eq. 2.36, page 65), where increased image resolution comes at the expense of loss of SNR.

The second property of x^2 is that it is non-bijective. This means that, except for $x = 0$, there are always two locations, which are mapped onto one single frequency. A measurement from a single coil is therefore not sufficient to uniquely determine the location of the signal origin. This ambiguity is similar to what is known from conventional accelerated parallel imaging

(cf. for example Fig. 2.10, page 76). In PatLoc, the encoding ambiguities are resolved with the help of several receiver coils with different sensitivity at the ambiguous locations. Note that after unfolding twice as many voxels are reconstructed. Correspondingly, the average image resolution is doubled. Fig. 3.2 motivates that signal discrimination is feasible with several RF-receiver coils.

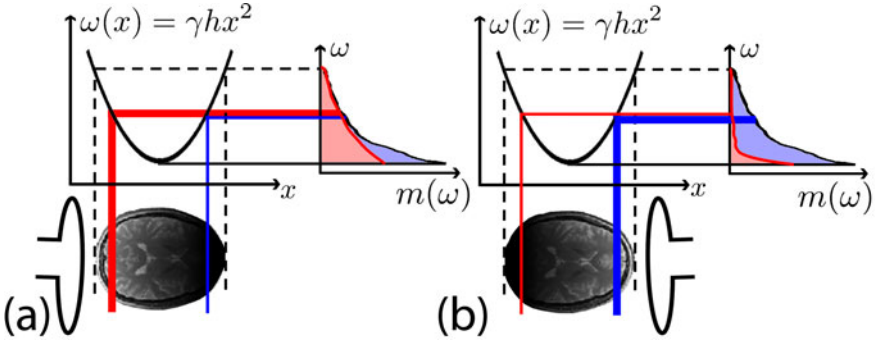

Figure 3.2: Determination of source locations with parallel acquisition. (a) and (b) show the situation for two RF-receiver coils with different spatial sensitivity. Coils (a) and (b) are sensitive on opposite sides of the example object. The signal paths are in red or blue color depending on from which side of vertex of the parabolic encoding field the signal emanates. The highlighted signal paths in (a) show that almost the complete signal energy originates from the left of the vertex, whereas the signal paths in (b) show that the opposite is the case for the second coil. For this particular frequency, the difference in RF-coil sensitivities therefore allows one to uniquely determine the locations of the signal sources. The signal plots indicate that this is also true for most frequencies. At the center, however, there is a significant sensitivity overlap and more insight into the problem is necessary to answer the question to what extent signal discrimination is possible.

These properties – non-homogeneous, but on average increased image resolution, spatially varying SNR, and the necessity to supplement encoding with RF arrays – are also inherent to 2D imaging with two NB-SEMs (see e.g. chapter 5.1, page 155ff), and typical if more than two SEMs are used for signal encoding (see e.g. chapter 7.2.2, page 255ff). These and other properties of NB-SEMs offer new degrees of freedom for MRI signal encoding. The next section gives examples how these new degrees of freedom can be exploited to develop interesting new applications for MRI.

3.2 Applications

3.2.1 Background: New Encoding Options

There are very good arguments to use linear gradient fields in MRI. These fields allow signal encoding in the Fourier domain of the object. For single-channel Cartesian acquisitions, image reconstruction is fast (FFT) and results in images with constant spatial resolution (cf. Eq. 2.33) and optimal, homogeneous SNR (cf. Eq. 2.36). These properties are very advantageous in many ways, yet not the only measure for diagnostic usability.

A good example is parallel imaging, where the homogeneous and optimal SNR properties of the reconstructed images are sacrificed in favor of imaging speed; many other useful applications have evolved with the development of PI. The main reason for this tremendous impact of PI has been the extension of encoding capabilities compared to single-channel acquisitions.

In this sense, PatLoc has a similar target: extending the encoding capabilities of current imaging hardware. This task is achieved by making the gradient system itself more flexible. This approach is promising because the gradients provide the major part of the overall encoding information. A PatLoc encoding system offers new encoding options by not restricting encoding to linear SEMs; curvilinear and non-bijective SEMs are also available for signal localization.

The relevance of PatLoc is augmented by the availability of parallel reception on many modern scanners. Reconsider that the additional information provided by an array of RF coils has shown that gradient encoding can be reduced to an extent, which would normally lead to non-unique encoding. PI therefore allows incomplete gradient encoding that can also be a consequence of non-bijective SEMs. Despite the various possibilities that PI offers to use non-complete gradient encoding strategies, the existing gradient hardware has remained the same, while the research concentrated on modifying k-space sampling schemes. In PatLoc it is reviewed whether modifications of the gradient system lead to more efficient signal encoding especially in the context of PI. Novel encoding strategies are investigated, adequate reconstruction methods are developed and new applications in medical diagnostics are explored.

Potential benefits of PatLoc were already discussed in the initial conceptual publication [[61]]. It was motivated therein that PatLoc is useful because it allows customization of the encoding fields to the underlying anatomical structures. Also, it has been hypothesized in [[61]] that the problem of peripheral nerve stimulation (PNS) could be reduced with PatLoc. Soon, it has been realized that PatLoc can be efficient in the context of RF reception [[156]] (low g-factor) as well as in the context of RF transmission [54, 152], [[191]] (shorter pulses, more efficient acquisitions of functional MRI data). Particularly interesting are the options, which PatLoc offers for reduced field-of-view imaging [[213, 207]]. One example is the elimination of balanced SSFP[1] banding artifacts [[206]]. PatLoc is still a very new technology. The wide range of possible applications is promising and the increasing interest in PatLoc and related approaches [178, 80, 98, 97, 93], [[100, 101]], will undoubtedly lead to many new and creative ideas for medical diagnosis. I have selected a few interesting applications, which are described in the following three sections in more detail.

3.2.2 Improved Encoding Efficiency

With modern gradient hardware a linear SEM can be switched fast and accurately. Moreover, the three available channels allow arbitrary spatial orientation of the linear SEM. However, there is no possibility to deviate from the linear geometry. One of the major incentives for the development of a PatLoc system has been the observation that alternative SEM geometries are often better adapted to the anatomical shapes of the measured objects. Also, alternative field geometries have different effects on technical as well as physiological restrictions. It is therefore to be expected that improvements in encoding efficiency can be achieved with PatLoc resulting in reduced scan times or increased diagnostic information. This aspect is further motivated in this section by discussing situations with increasing flexibility; a single SEM, then two SEMs and finally more than two SEMs are considered.

Encoding with One SEM As an example, consider the MR-Encephalography project [64, 69, 211]. The aim of this project is to map brain physiology with a maximum temporal resolution. Image resolution on the other hand

[1] Acronym for *Steady-State Free Precession*. More information on balanced SSFP imaging sequences can be found in [53], page 796.

is not of major interest. In this context, the idea came up to encode with only one gradient coil and replace the encoding of the second gradient coil entirely by RF-sensitivity encoding (also cf. [[61]]). This approach would significantly lower the achievable image resolution. On the other hand, the signal acquisitions would be much faster because slow sequential gradient encoding would be replaced by fast simultaneous RF-sensitivity encoding. In this situation, the question arose if a linear encoding field is really always the optimal choice; in cortical imaging for example, information is required from the periphery of the brain only. However, linear gradient fields also encode the center of the brain and, due to the rectangular shape of the fields, also significant parts outside of the brain are encoded. In this situation, elliptical encoding fields would be better suited because the geometrical shape of these fields would cause magnetic field variations to be significant almost exclusively within the region of interest. This claim is supported by Fig. 3.3.

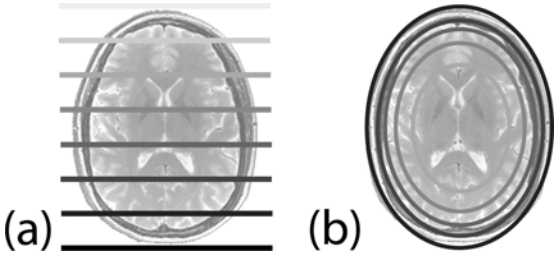

Figure 3.3: Encoding with one SEM. An example for cortical imaging. (a) Encoding with a conventional linear gradient field (field isolines are shown). (b) Efficient depth-encoding with elliptical SEMs having a high spatial derivative at the periphery. For cortical imaging, it is important to retrieve information from the periphery of the brain. In fast imaging modalities, where a gradient is used only for depth-encoding, and encoding along the circumferential direction is done with RF coils, elliptically-shaped encoding fields are better adapted to the anatomy of the cortex than linear fields.

Encoding with Two SEMs Not only ultra-fast imaging modalities, where a single gradient field is used, would profit from optimized field designs. Also encoding modalities, where two SEMs are used for in-plane imaging profit from the additional flexibility that PatLoc offers. In the 1D example of Fig. 3.1, it is motivated that image resolution depends on the spatial derivative of the encoding fields. The dependency of image resolution to the field derivatives can be exploited in the following way: Suppose that not the

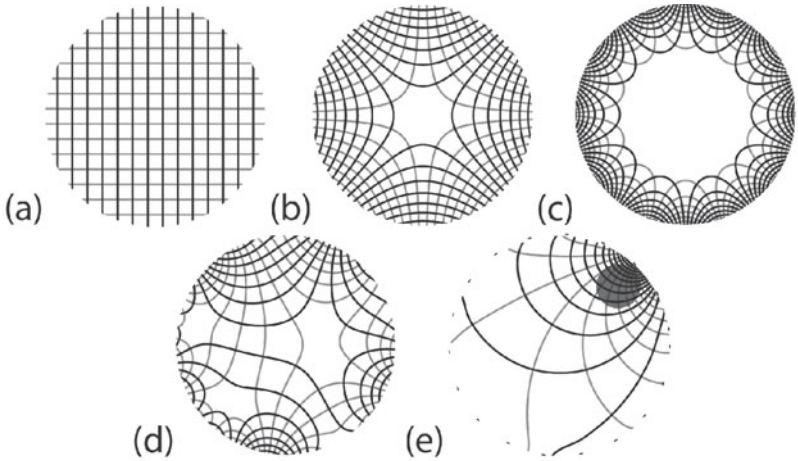

Figure 3.4: Contour plots of several orthogonal hypothetical SEMs. Size and shape of the small areas between the contour lines reflect the local image resolution. (a) Standard linear SEMs have homogeneous resolution. (b) For quadrupolar SEMs, there is a clear resolution gradient toward the periphery. Note that with the same number of isocontour lines (i.e., for the same amount of acquired data), there are twice as many voxels compared to linear encoding fields. (c) For multipolar SEMs with even higher polarity, the number of voxels is higher, however, also the resolution gradient is more pronounced. (d) Shown is an arbitrary SEM. It has an almost arbitrary resolution pattern. At the periphery, a tendency toward an increased image resolution is visible. (e) Especially for ROIs at the periphery (gray circle), encoding can be highly efficient if optimized for those ROIs only.

whole object, but only a sub-volume is important for a certain measurement. Then, fields with strong spatial derivatives are required for this sub-volume and outside of this region it is sufficient to have flat field geometries. PatLoc can be used to design SEMs such that encoding is more efficient in the ROI while restricting loss of encoding efficiency to regions of minor interest. For more homogeneous resolution inside the ROI, a method has been developed, which allows one to partially homogenize image resolution by sacrificing some of the abundant SNR of the low-resolution image parts [[190]]. A nice way of visualizing image resolution is to plot contour lines of both encoding fields on top of each other. Some theoretical examples of different orthogonal field geometries are shown in Fig. 3.4.[2] These examples show

[2]Consult Appendix A.4, page 299ff, for an elegant way of describing orthogonal fields in 2D with complex-valued analysis. More information is found in [[159]].

that there is a high flexibility in field design. Even more flexibility exists when the requirement of orthogonality is relaxed.

The quadrupolar field design, which corresponds to Fig. 3.4b, has been realized experimentally (see section 3.3, page 121ff). If those fields are used instead of the linear encoding fields, the encoding efficiency differs throughout the image. Because of the nonlinearities, almost no information of the image is encoded at the center, whereas at the periphery, a high resolution results (cf. Fig. 3.5). Analogous to the 1D example of section 3.1, page 103ff, the non-bijectiveness of the fields is responsible for a doubling of the average image resolution compared to standard gradient encoding for the same amount of acquired data.

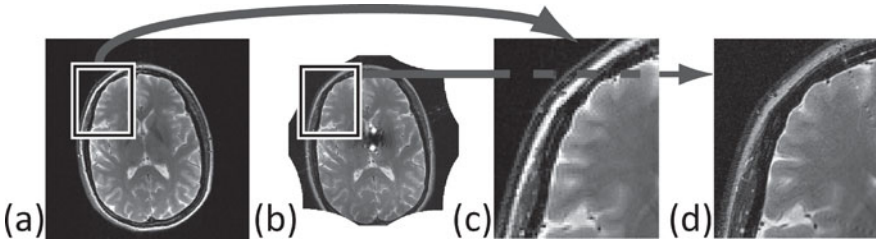

Figure 3.5: Image resolution with quadrupolar SEM encoding. (a) With standard linear gradient fields image resolution is homogeneous. (b) With quadrupolar SEMs, almost no image information is available at the center. Image resolution improves however toward the periphery. Some pronounced streaking artifacts are visible, which originate from the center. (c) and (d) Comparison of two similar zoomed-in sections show that image resolution is indeed higher with PatLoc within the peripheral region. Both images have been acquired with the same imaging parameters to allow fair comparison.

The contour plots shown in Fig. 3.4 and the experimental results shown in Fig. 3.5 reveal that encoding is typically more efficient near the coil surfaces (at the periphery). The reason for this property is obvious: The influence of the currents in the coils decreases with increasing distance. Especially at the periphery, there is room to improve the encoding efficiency as indicated by Fig. 3.4e.[3] Hence, a more flexible field design would profit from coil arrangements, which can be adapted to the anatomical shape of the imaged

[3]The example shown in subfigure (e) has been found using complex-valued analysis (cf. Appendix A.4, page 299ff) by minimizing $|f'(s)|$ (f and s are defined here as in Appendix A.4) outside of the ROI under the constraint that $(\sum_{s\in ROI} |f'(s)|^2)^{1/2}$ is constant within the ROI. Note that $|f'(s)|$ is equivalent to the Jacobian determinant of the corresponding

part of the body. In summary, an encoding system with two NB-SEMs of adequate geometry is useful to locally improve image resolution or to accelerate image acquisitions. The effects are enhanced considering that an intrinsic acceleration is associated with non-bijective encoding.

Encoding with More than Two SEMs It is clear that effective field design is only possible with a flexible encoding system. Such a system would preferably consist of a large amount of coil channels. In Freiburg, a six channel system has recently been established, which allows simultaneous switching of the three linear channels and the two quadrupolar SEMs [[42]]. Also, a planar three-channel coil is currently being tested [[103]]. In the future, efforts will be focused on the development of a much more flexible multi-channel system.

The variations in image resolution resulting from such multi-channel systems depend not only on the field geometry, but also on the chosen time courses of the coil currents. The impact of such multi-dimensional encoding strategies on image properties like image resolution is therefore much more complex than if only two SEMs are involved. The local k-space concept, developed by Dr. Daniel Gallichan, has proven very helpful in this regard. The idea of local k-space has fruitfully been used to design and analyze complex multi-dimensional trajectories [[42]]; moreover, it is useful in related topics like GradLoc [[207]]. A discussion of this important concept should therefore not be spared, and is explained with further detail at the end of this section.

An interesting example in the present context is the 4D-RIO[4]-trajectory [[42]] that makes use of linear SEMs as well as NB-SEMs. On the one hand, images encoded with this multidimensional (4D) trajectory have properties that resemble those which are typically associated with linear gradient fields; for example, an extended portion of the image exhibits a homogeneous resolution (cf. Fig. 7.12, page 265). On the other hand, fundamental differences to conventional imaging arise; for example, image contrast is heavily affected by the 4D encoding.

---

two-dimensional real-valued vector field and thus approximates image resolution very well (cf. chapter 5.1.1e, on page 169, in combination with Eq. 5.8).

[4] Acronym for *4-Dimensional Radial In/out vs. Out/in*. This trajectory is briefly presented in chapter 7.2.1b, page 254f.

4D-RIO illustrates the capabilities of multi-dimensional trajectories to create new imaging effects, made possible by the additional spatial and temporal degrees of freedom that become available to redefine the magnetic field evolution within the measured object. These additional degrees of freedom may also be exploited to reduce scan time; to understand this, it is crucial to note that any encoding strategy is subject to many different limitations. There are restrictions of technical nature. For example, the SEMs cannot be switched infinitely fast because the coils that generate the SEMs have a finite inductivity. Also, there are restrictions of physiological nature, notably peripheral nerve stimulation caused by switched magnetic fields. These technical and physiological restrictions have the effect that there is a minimum execution time associated with a particular encoding strategy. One encoding strategy can be faster, i.e., more efficient, than a different strategy. Multi-dimensional PatLoc trajectories offer the possibility to design fast encoding strategies that are less demanding for certain restrictions than if encoded with purely linear SEMs, without necessarily having to cut back on relevant image information (like for example image resolution in the ROI).

The relationship between restrictions and encoding strategy is very complex and far from being understood. A thorough analysis of this important topic is still to be undertaken. In the following section, after a short note on local k-space, at least qualitative arguments are presented which show that NB-SEMs have the potential to reduce the problem of peripheral nerve stimulation.

The Concept of Local k-Space The concept may be understood by comparing it to standard k-space. Recall that k-space corresponds to the space of encoded *spatial frequencies*. When k-space is sampled, different spatial frequencies of the object are acquired. The achieved image resolution is related to the highest sampled spatial frequencies, and aliasing occurs if the distance between the sampled spatial frequencies is too high (cf. paragraph *Field-of-View* on page 62ff in chapter 2.2.1c). In contrast to conventional imaging, where the spatial frequencies of the encoding functions do not change throughout the image, in PatLoc, each location encounters modulations with different spatial frequencies during the acquisition process. Therefore, each position has its own local distribution of encoded spatial frequencies; these local spatial frequencies define the spatial information that is available about the measured object at each location; in other words:

the encoded information at location $\vec{x}_\rho$ is defined by the distribution of the *local* k-space variable:

$$\vec{k}_{loc}(\vec{x}_\rho, t) := (\nabla\phi)(\vec{x}_\rho, t). \tag{3.1}$$

Here, $\phi(\cdot)$ represents the encoded phase distribution at location $\vec{x}_\rho$ at time-point t, and $\nabla\phi$, the corresponding local spatial frequency distribution. Some examples of local k-space distributions are depicted in Fig. 3.6.

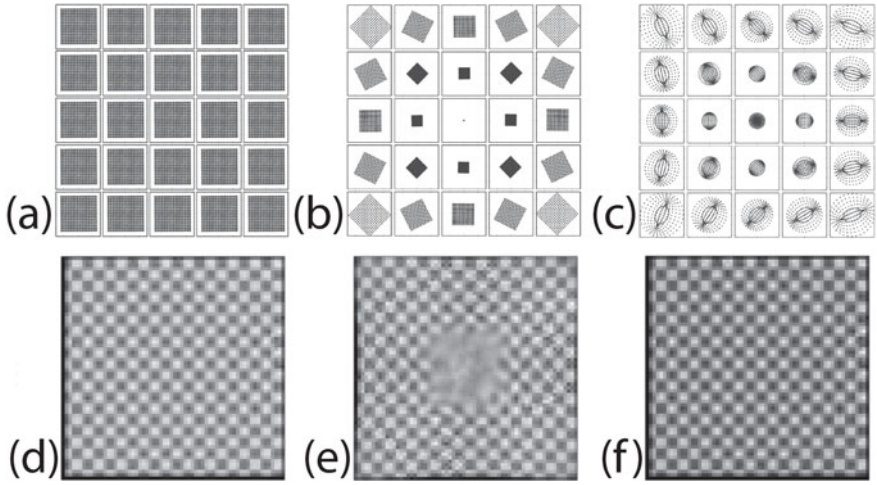

Figure 3.6: Local k-space (a-c) and examples of corresponding reconstructed images (d-f). (a,d) Conventional imaging. Local k-space is the same everywhere. Therefore, image resolution is constant throughout the image. (b,e) PatLoc imaging with two orthogonal quadrupolar SEMs. At the periphery, local k-space is enlarged, whereas it collapses to a single point at the center. Correspondingly, image resolution is high at the periphery, whereas it degrades toward the center. (c,f) Complex 4D trajectory, where linear and quadrupolar fields are involved. The trajectory is the 4D-RIO trajectory presented in [[42]]. The extent of local k-space is more evenly distributed compared to the pure quadrupolar PatLoc example. Therefore, also image resolution does not deteriorate toward the center (also see Fig. 7.13, page 267). The images are courtesy of Dr. Daniel Gallichan. Similar images have been published in [[42]].

The figure also illustrates that the extent of local k-space is closely related to the local image resolution. This observation can also be substantiated by theoretical means as shown in Appendix A.5.1, page 303ff. This shows that the relation between k-space extent and image resolution, that is well-

known from conventional imaging, can immediately be adopted on a local level as well. Interestingly, this is not possible for the aliasing artifact: From the local sampling density alone no precise conclusions concerning aliasing at a certain location can be drawn because the aliasing artifact is not a local effect. Also note that, in the basic formulation of the concept, supplementary RF encoding is disregarded.

In the context of PatLoc imaging, it is particularly useful to link local k-space to what is actually done in the experiment. The exact relationship between the user-defined PatLoc acquisition trajectory and local k-space distribution is presented in Appendix A.5.2, page 305f, and illustrated for the three examples of Fig. 3.6.

3.2.3 Reduction of Peripheral Nerve Stimulation

A problematic side-effect of gradient switching is the possibility of peripheral nerve stimulation. PNS is a physiological reaction often perceived as a tingling sensation. It can, however, also cause significant pain and in the worst case, cardiac arrest might be triggered [46]. Gradient technology has advanced significantly in terms of field strength and switching rate, such that PNS has become a patient safety issue on many modern MR systems. This implies that nowadays gradient trajectory performance is often not restricted by gradient technology, but rather by physiological restrictions. The PatLoc approach offers possibilities to speed up the encoding process without exceeding the PNS limits. To understand this, a quick review of the causes for PNS is given in the next two paragraphs. A detailed presentation of this topic with further references is found in [46].

The term *peripheral nerve stimulation* correctly reveals that involuntary *nerve activation can be triggered* by switched gradients, i.e., by magnetic fields, which vary in the audio-frequency range. PNS is not a direct magnetic effect because it is a well-known fact from electrophysiology that nerve activation is triggered by the electric field and not the magnetic field itself [46]. However, basic electromagnetic theory states that an electrical field is generated by a time-varying magnetic field and therefore also a switched gradient field can cause nerve stimulation. More concretely, the integral of the electric field along a certain path (= voltage) is proportional to the time derivative of the magnetic flux flow through an enclosed area (Faraday's law): $\oint \vec{E} d\vec{l} = \iint \dot{\vec{B}} d\vec{A}$. Consider now a simple an idealistic situation

[144], where the human body is modeled as a cylinder with homogeneous tissue parameters and where the encoding field is assumed to have a pure constant gradient in the z-direction.[5] It can easily be shown that under these assumptions, the above equation has the solution: $E \propto r \cdot dB/dt$, where r is the distance from the z-axis. From this equation, it can be concluded that the current flows inside the human body are proportional to dB/dt. And indeed, stimulation occurs primarily at the periphery of the body like shoulders and arms [33], where dB/dt is typically very high. However, the currents are also proportional to the size r of the current loops. This is the main reason, why patients should avoid folding their hands during a scan [38].

The model is especially useful to predict current flows in the human body. These current flows can lead to nerve stimulation. It has been observed and analyzed a long time ago by Weiss and Lapicque [195, 89] that currents must flow for a certain amount of time τ to build up sufficient potential differences to cause cell depolarization. Irnich et al. have shown in [71] that the stimulation model of Weiss and Lapicque can be combined with the model presented in the previous paragraph. They derive a formula (Eq. 9 in [71]), which is of particular interest also in the context of PatLoc imaging, for the minimum magnetic field strength $B(\tau)$ required to cause nerve stimulation: $B(\tau) = B_{min} \cdot (1 + \tau/\tau_c)$. In this formula, τ can be interpreted as the pulse duration, τ_c is the chronaxie [89], a tissue dependent time constant, and B_{min} is the minimum, physically not realizable, instantaneous field change required to cause stimulation. Apart from the dependency on pulse duration, the formula is very interesting because it suggests that it is rather the absolute value of the peak-to-peak magnetic field change, which matters and peak dB/dt is not of primary interest. This result has been substantiated in [71] and also the results evaluated from different publications [33] support the claim that it might be reasonable for legal regulations to determine switching limits rather on B itself than on dB/dt.

Why is this interesting in the context of PatLoc? Consider Fig. 3.7. In this figure, a switched quadratic gradient is compared to a switched linear gradient. The comparison of Fig. 3.7a with Fig. 3.7b shows that the non-bijectiveness of the fields can indeed lead to reduced peak-to-peak magnetic field variations during switching. Note that the reduction depends on

[5] In reality, a gradient field is necessarily accompanied by concomitant field components (cf. e.g. [9]; also see chapter 1.2.2, on page 28).

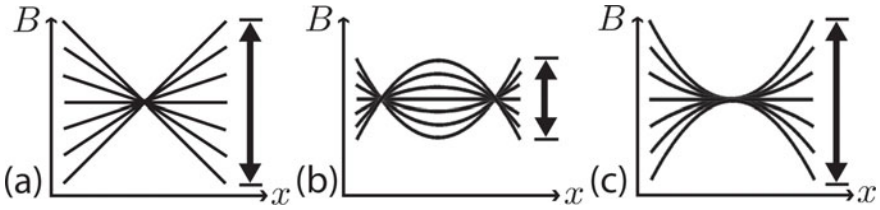

Figure 3.7: PNS in PatLoc: a 1D example. (a) Shown is a linear gradient field, which is switched from one extreme to the other. (b) The peak-to-peak variation is halved for a quadratic encoding field. This has beneficial consequences for PNS. Note that the average encoding efficiency, given by the derivative of the SEM, is preserved. (c) Care must be taken how the switching is performed, otherwise no gain might result.

how the fields are actually switched. If they are switched as indicated in Fig. 3.7b, the amplitude is halved; if, however, switched as in Fig. 3.7c, the amplitude is the same! It is clear that the 1D example of Fig. 3.7 can only give a rough understanding about the PNS capabilities of practical PatLoc measurements. Concomitant fields must be considered and, what is even more intricate, it is important to consider that the different geometric shapes of the encoding fields influence the non-local effects (for example current loops, influence of differing tissue properties), which are important for PNS. Initial investigations have been performed to ensure that safety margins are not exceeded by the used experimental setup [[24]]. This was necessary to get ethical approval from the Ethics Commission of the University of Freiburg. Further investigations with more flexible SEM systems are indispensable to evaluate the PNS capabilities of PatLoc under realistic conditions. This will also involve patient studies and therefore safety considerations will be of primary importance in this regard.

3.2.4 Applications Involving Nonlinear Phase Preparation

Particularly promising are applications with nonlinear phase preparation added to conventional gradient encoding. Nonlinear phase preparation is a method, where a nonlinear PatLoc-SEM is switched before signal reception. The nonlinearity of the SEM causes signal echoes to be formed at different time points, depending on the location of the signal source. This spatio-temporal correlation of echo formation is exploited by a method that has been termed *GradLoc* to perform reduced FOV-imaging [[213, 207]] and by

STAGES[6] [[206]] to enhance the homogeneity of the B_0 field during signal acquisition. The lion's share for the development of these two applications can be attributed to Dr. Walter Witschey. Relevant prior art is referenced and briefly discussed in the above publications. The basic ideas and initial results are reviewed in this section. For simplicity, only SEMs with quadratic terms are considered for phase preparation.

a) GradLoc: Reduced Field-of-View-Imaging

In conventional imaging, the k-space signal energy is typically focused at the center of k-space (echo). This behavior changes dramatically, when a quadratic SEM is applied during phase encoding in addition to the linear gradients: The k-space echo spreads out over a region that becomes larger with increasing field strength of the quadratic field. This effect is often denoted as *phase-scrambling* (also see [131]) and is illustrated in Fig. 3.8. This figure also reveals an astonishing property of quadratic phase preparation: With increasing quadratic phase, the k-space progressively resembles the actual image. When the quadratic field is increased even further, parts of the echoes leave the acquired region and, consequently, peripheral parts of the image are cropped (also visible in Fig. 9d in [72]), whereas the central part of the image remains almost unaffected.

What is the reason for this strong correlation between image space and k-space? Recall that in conventional imaging, the gradients impose a phase $\phi \propto kx$ onto the magnetization, where k is the k-space variable and x is the source location.[7] The quadratic SEM is responsible for an additional phase accumulation proportional to αx^2 resulting in the overall phase of $\phi \propto (k + k_q(x))x$, where $k_q(x) = \alpha x$. Quadratic phase preparation therefore leads to a splitting of the echo into individual components, where the echo of each source location x is not centered around $k = 0$, but shifted to $-k_q(x) = -\alpha x$. Most signal energy of each individual component is therefore located at $-\alpha x$ in k-space. This is the reason for the one-to-one correspondence of k-space signal echo shift and image space source location and why (a) k-space and reconstructed image look similar and why (b) for large values of α, those parts of the reconstructed image vanish which correspond to k-space values that have been shifted outside of the acquired

[6] Acronym for *Steady-STAte Gradient Echo Shimming*.

[7] The explanation is in 1D. It can be extended to 2D and 3D in a straightforward manner [[207]].

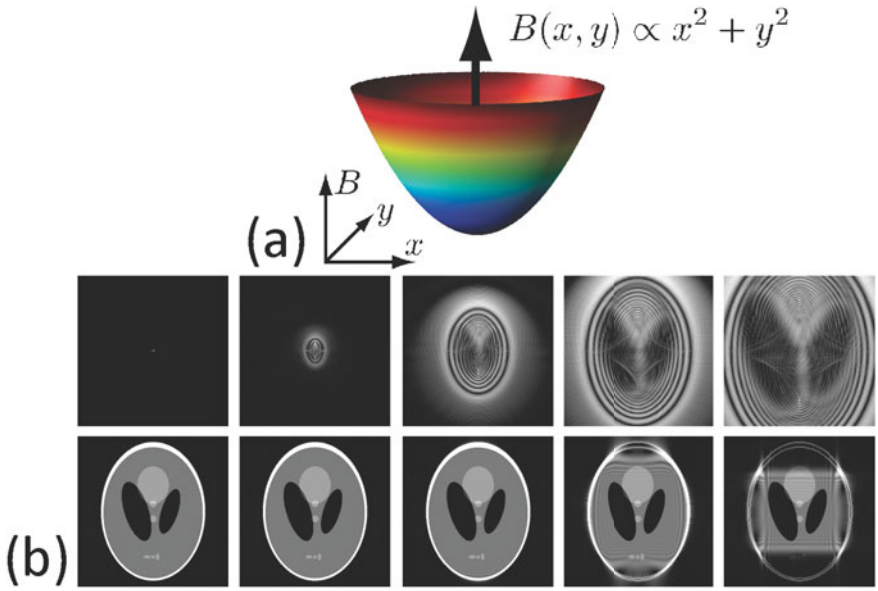

Figure 3.8: Effect of quadratic phase preparation. (a) Geometry of a 2D quadratic encoding field. (b) Bottom: Reconstructed image. Top: Corresponding k-space signal. From left to right: Without phase preparation, there is a single central k-space echo. With increasing quadratic phase, the echoes originating from different parts of the object separate. For large quadratic phase, peripheral echoes are not acquired anymore and signal loss in the reconstructed images occurs. According to the square-shaped acquisition window, the shape of the localized image is also square-shaped. Some residual aliasing from high-frequency components remains visible.

k-space region. More precisely, if the k-space region K has been acquired, only those parts of the image are visible, which lie in the region $V \propto \alpha K$.

This relation is also valid in 2D and 3D [[207]] and has a direct application: The user can select a ROI V within the object, perform standard imaging supplemented with quadratic phase preparation, and acquire the k-space region with the same shape as the ROI: $K \propto V/\alpha$. This procedure allows reduced FOV-imaging because the fold-over artifacts otherwise encountered along the phase encoding direction (Fig. 3.9a) are avoided. A similar result may be found with selective excitation pulses. Such pulses are, however, typically long and often a significant amount of energy is deposited in the measured objects. These negative effects are avoided with GradLoc.

Note that the localized boundary in V is not perfectly sharp. The reason for this unwanted effect is that most, but not all signal energy is located at the center locations of the individual echoes. High-frequency information may result in artifacts, for example some residual artifacts are visible outside of the localized square in Fig. 3.9a. Surprisingly, these artifacts do not seem to be problematic under in vivo imaging conditions (see Fig. 3.9b).

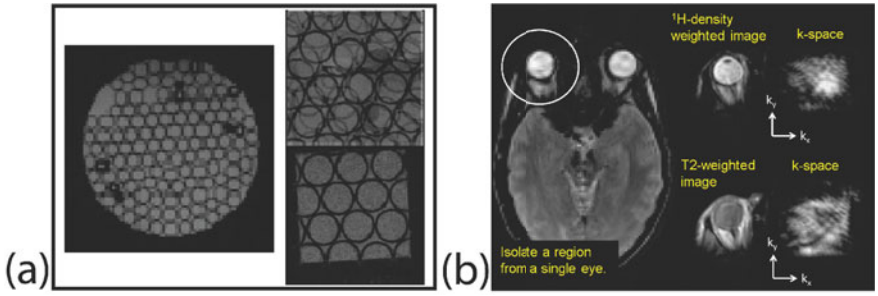

Figure 3.9: GradLoc measurement results. (a) Phantom measurements. Left: No aliasing occurs with full k-space sampling. Right, top: Undersampling along the vertical direction results in the typical fold-over artifact. Right, bottom: With a quadratic phase, a high-resolution image without aliasing results. (b) These advantages are also visible under in vivo conditions. Note the comparably weak high-frequency artifact compared to the simulations in Fig. 3.8. The images are courtesy of Dr. Walter Witschey. The images in (a) have been taken from [[205]] and the image in (b) was part of the corresponding poster presentation at the ISMRM conference 2011 in Montreal. The phase of the acquired data was prepared with a quadrupolar SEM provided by the available PatLoc hardware. This SEM and the quadratic SEM used in Fig. 3.8 both result in linear k-space echo shifts and are therefore equivalent in the context of GradLoc [[205]].

b) STAGES: Dynamic Intra-Slice Shimming

STAGES [[206]] is a novel dynamic shim updating technique; similar to GradLoc, it is based on the localization properties resulting from nonlinear phase preparation. Shimming comprises methods to enhance the homogeneity of the B_0-field, which is perturbed by susceptibility differences between tissue borders. Active shimming is typically performed with a set of shim coils that are designed to generate the lowest orders of solid harmonics. Shimming may be divided into static shimming and dynamic shimming methods. In static shimming, B_0-inhomogeneity maps are acquired and the currents in the shim coils are adjusted before the actual measurement

to optimize the shim for the whole excited region or also for a particular ROI. In dynamic shimming, several shim updates are performed during the acquisition. A problem with existing shimming methods is that they are restricted to shimming between successive excitations; i.e., the shims may be updated from slice to slice. It is however not possible to shim during the acquisition of a single slice if encoding is done with only linear gradients. That is, where STAGES comes into play: It is possible to perform not only *inter*-slice shimming, but also *intra*-slice shimming.

This is possible because of the k-space relocalization properties of the nonlinear phase preparation. Recall that k-space is actually traversed in the temporal domain along a user-defined k-space trajectory (cf. chapter 1.2.2, page 27ff). Relocalization of MR signals in k-space is therefore, from the perspective of the concrete measurement, a temporal rearrangement of the individual MR echoes, which originate from different locations of the measured object. In the previous section, where GradLoc is explained, it is shown that a quadratic SEM leads to a one-to-one correspondence of k-space and source location. In the temporal description this means that at each instant of time, signal echoes are recorded, which originate from a very localized region *within* the excited slice. Thus, it is possible to optimize the shim for that localized region only. While traversing k-space, the region that contributes signal changes. It is therefore possible to update the shims to the currently contributing region with the consequence of significantly enhanced image quality. Note that such an *intra*-slice shim updating protocol requires a nonlinear SEM. With linear SEMs, the signal echoes occur all at the same time. Therefore all image parts are equally affected by the shimming parameters. If these are optimized at one instant for a certain region, the quality may be enhanced at that location, however, only at the expense of image deterioration elsewhere. This problem is avoided with nonlinear phase preparation.

The dynamic shimming capabilities have been demonstrated for a problem, which is known to result from B_0-inhomogeneities: In balanced SSFP sequences (cf. [53], page 796), banding artifacts with unwanted signal loss occur (see Fig. 3.10a). Fig. 3.10b shows that these banding artifacts could be eliminated with STAGES. More information about the concrete update scheme and the used sequence parameters is found in [[206]].

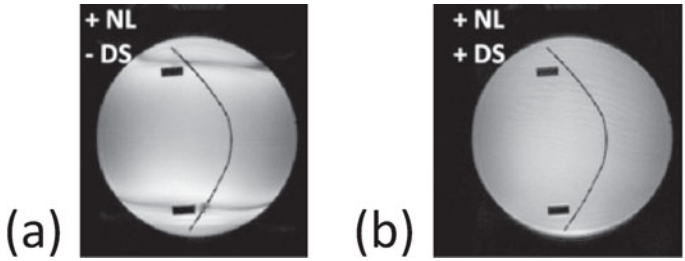

Figure 3.10: Banding artifact suppression with STAGES. (a) Images acquired with balanced SSFP sequences are typically corrupted with such a banding artifact. (b) With STAGES this artifact is eliminated. The images are courtesy of Dr. Walter Witschey and have been taken from [[206]].

3.2.5 Summary

These examples show that PatLoc has potential benefits in various areas of MRI. Some of these benefits could already be verified with the current PatLoc hardware, others still wait for ethical approval to be evaluated. Some benefits like improved encoding efficiency call for a more flexible gradient system. PatLoc is still a young imaging modality with many open questions. It is very probable that further investigations will create new ideas about how the gained flexibility in signal encoding can be used to solve current problems in MRI and generate new applications for medical imaging.

3.3 Initial Experimental Setups

In this section, the first two hardware designs of a PatLoc imaging system are presented that were constructed during the course of the PatLoc project. Another, high-performance system is currently being installed and is not presented here. The first PatLoc prototype coil has been built to fit into a 9.4 T BioSpec research system for small animal MRI (Bruker BioSpin MRI GmbH, Ettlingen, Germany). The second PatLoc coil was constructed significantly larger as an insert coil for human head imaging on a MAGNETOM Trio, A Tim System 3 T (Siemens Healthcare, Erlangen, Germany). Both PatLoc gradient coils were designed to generate two orthogonal quadrupolar encoding fields. These fields are introduced in the following section before the animal and the human systems are presented in more detail.

3.3.1 Multipolar Encoding Fields

The orthogonal quadrupolar SEMs realized in the experiments form special types of orthogonal multipolar SEMs [[63]]. These two fields are best described in polar coordinates, where they are represented by $\psi_1(r,\varphi) \propto r^L \cos(L\varphi)$ and $\psi_2(r,\varphi) \propto r^L \sin(L\varphi)$. The fields of lowest order $L = 1$ are just the standard x- and y-gradients. The fields with $L = 2$ are the quadrupolar fields which are generated with the custom-made PatLoc hardware. The field geometry of the two quadrupolar fields is shown in Fig. 3.11; it is equivalent to the geometry of the fields generated by shim coils of order $(L := 2, L := 2)$.

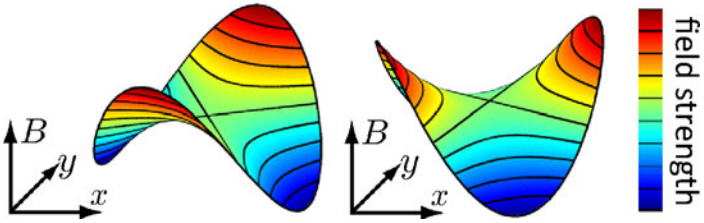

Figure 3.11: Quadrupolar SEMs. The two orthogonal quadrupolar SEMs form hyperbolic paraboloids, which are rotated against each other by $45°$. They are flat at the center and the field strength increases quadratically in the radial direction. Along the circumferential direction, the field changes sinusoidally with two poles on opposite sides of the center.

Both fields are also orthogonal to the z-gradient $\psi_3(\cdot) \propto z$. Orthogonality means in this case that the gradients of the magnetic fields are perpendicular. The orthogonality of the fields can easily be computed by verifying that $(\nabla\psi_i) \cdot (\nabla\psi_j) = 0$ for all $i \neq j$. Orthogonal multipolar SEMs have the remarkable property that appropriate combinations of them generate *all feasible* magnetic encoding fields under the condition that the gradients of these two fields plus the z-gradient are globally orthogonal to each other. This statement is proven in Appendix A.4, page 299ff. One important result of the proof is that it identifies the linear gradient fields as the most basic encoding fields, followed by orthogonal quadrupolar SEMs. From this mathematical point of view, the realized PatLoc hardware is the first and most basic step toward encoding fields with a virtually arbitrary geometry, and PatLoc imaging can be regarded as a natural generalization of standard Fourier imaging.

The requirement of orthogonality is not a necessary condition for imaging, however, it ensures maximal encoding efficiency because encoding along orthogonal directions adds complementary information, whereas encoding along the same direction does not yield new information. Fig. 3.12 illustrates that the angle of encoding directions has consequences for the shapes of the voxels and therefore also for image resolution. Within the accuracy of the voxel model as used in the figure, the voxels form parallelograms for linear SEMs whose area is given by $f = |(\nabla\psi_1)| \cdot |\nabla\psi_2)|/\sin(\phi)$, where ϕ is the angle between the gradient fields of the two SEMs. For given field strengths, image resolution is therefore maximized when the field gradients approach orthogonality. Another advantage of orthogonal SEMs is that the voxels form compact squares instead of anisotropic parallelograms. For small voxels, the same is true for nonlinear SEMs.

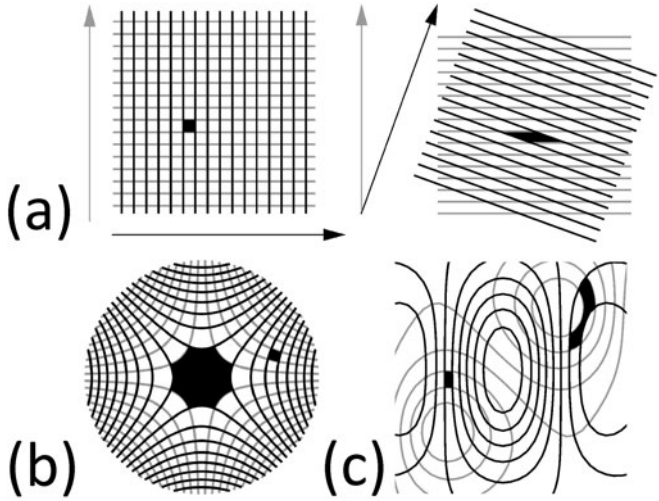

Figure 3.12: Voxel shapes and local encoding directions. (a) Two linear SEMs. Left: Orthogonal SEMs. Right: Non-orthogonal SEMs. The areas enclosed by the contour lines roughly approximate size and shape of the voxels within the reconstructed images. Within this approximation, voxels have the highest quality with orthogonal encoding directions. (b) At the periphery, an optimal voxel shape is preserved with quadrupolar orthogonal SEMs. Only at the center, deviations from the optimal shape are visible. (c) The shown example of two nonlinear SEMs illustrates that the angle of the encoding directions is an important parameter in determining the image quality also for the case of general nonlinear SEMs.

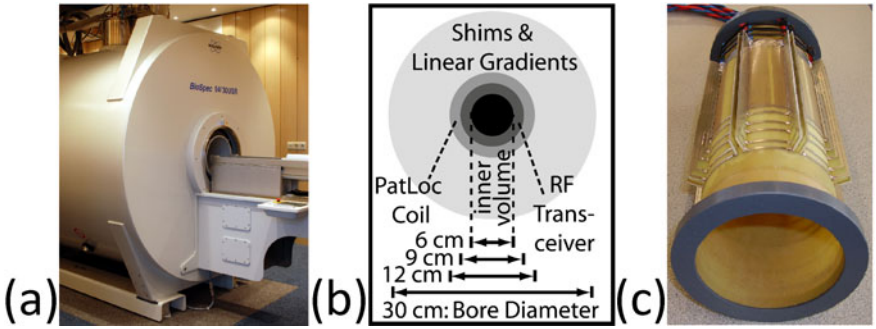

Figure 3.13: Experimental setup of the first PatLoc measurements. (a) The measurements were performed on a Bruker BioSpec 94/30 USR system. (b) From the $30\,\mathrm{cm}$ of the scanner bore only $12\,\mathrm{cm}$ could be used for the PatLoc insert and $6\,\mathrm{cm}$ were available for the measurements. (c) The PatLoc coil was manufactured manually based on an optimized octagonal wire topology. The optimal field geometry was between the 3rd and 4th rung at the opposite side of the cabling.

Note, however, that the voxel volume is for example only diminished by $13\,\%$ when the field directions form an angle of only $60\,^\circ$ with each other: The sinusoidal relationship of voxel size and angular encoding directions has the consequence that fairly large deviations from orthogonality can be tolerated in practice without a strong impact on encoding efficiency and image quality. Deviations from exact orthogonality can even be useful; for engineering reasons, but also from a theoretical perspective. For example, it might be useful to flatten out the multipolar fields toward the edges because the volume very near to the coil surface can often not be used for imaging and strong gradients in regions not being covered by the object should be avoided in order to guarantee a high level of encoding efficiency.

3.3.2 Animal System

The very first PatLoc experiments were performed on a $9.4\,\mathrm{T}$ BioSpec system for preclinical MRI (Bruker BioSpin MRI GmbH, Ettlingen, Germany, see Fig. 3.13a). The basic experimental setup has been presented in [[199]]. The results relevant to this thesis are reviewed here and information is added where necessary. The scanner bore had a diameter of $30\,\mathrm{cm}$, but only a volume of $6\,\mathrm{cm}$ in diameter could be used for phantom measurements because several hardware components like standard gradient hardware and

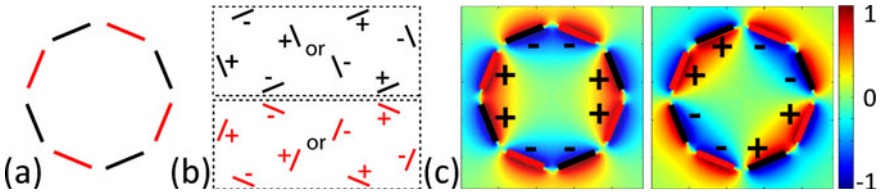

Figure 3.14: Generation of quadrupolar SEMs with the small-bore PatLoc prototype coil. (a) Two times four elements were connected with each other. (b) The four elements from each group were driven with alternating currents, which could flow in both directions. (c) One quadrupolar SEM was generated by driving both groups with equal currents. The second, orthogonal SEM was produced by reversing the current direction in one of the two element groups (shown is a slice at $z = 0$). The two quadrupolar fields could therefore be switched independently with the same controller normally used for the x- and y-gradients.

PatLoc coil insert used up the space in between. A cross section through the coil arrangement inside the scanner bore is depicted in Fig. 3.13b.

The PatLoc coil itself is shown in Fig. 3.13c. The coil was constructed manually with a length of $35\,\mathrm{cm}$ from which only about $6\,\mathrm{cm}$ could be used for imaging. The wire arrangement was based on a topology that had already been used for PatLoc simulations before [[61]]. The coil consisted of eight identical elements, arranged in an octagonal structure. In the simulations, the individual elements had imitated the symmetric design published in [21]. For the prototype coil, this design was optimized based on the method presented in [[105]] and for practical reasons, an asymmetric design was chosen for the individual elements with the current return paths all on the same side of the coil (cf. Fig. 3.13c).

In order to get two orthogonal quadrupolar SEMs, the eight elements were divided into two groups. Each group consisted of four elements, which were connected as shown in Fig. 3.14a. The first quadrupolar field was generated by applying equal currents in both element groups. The second quadrupolar field was generated by applying currents with reversed direction through the second element group. This procedure is depicted in Fig. 3.14b,c. The PatLoc coil could therefore be integrated into an existing hardware environment and the two channels, normally used for the switching of the x- and y-gradients were used to switch the two orthogonal quadrupolar SEMs instead. Fig. 3.15 shows that the design of the PatLoc prototype coil generated SEMs that were fairly similar to the exact quadrupolar coun-

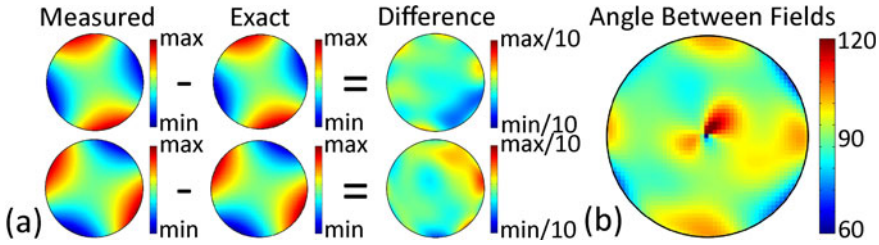

Figure 3.15: PatLoc SEMs generated by the small-bore prototype coil. (a) Top row and bottom row show the two different quadrupolar SEMs. On the left, measured PatLoc fields are shown. From these fields, exact hyperbolic paraboloids are subtracted resulting in a difference map. This map indicates that the true SEMs deviate from the exact counterparts by up to $10\,\%$ referred to the maximum field strength at the edge of the FOV. (b) Distribution of the angles between the two encoding directions. Note that all angles are between $60\,^\circ$ and $120\,^\circ$ indicating fairly high encoding efficiency.

terparts, at least in the central slice. In the relevant volume, the encoding directions were always between $60\,^\circ$ and $120\,^\circ$, which is sufficient to ensure efficient encoding in the whole volume of interest (see last paragraph of the latter section 3.3.1, on page 124).

One of the first images acquired with this hardware is shown in Fig. 3.16a. Signal data of a kiwi fruit were acquired with a 128×128 spin echo sequence ($TE = 50\,\mathrm{msec}$, $TR = 2\,\mathrm{sec}$). For the reference measurement the same parameters were used. The most obvious difference between the two images is the resolution gradient toward the outer parts of the kiwi fruit in the PatLoc image. Considering that the PatLoc prototype coil could only be driven with a maximum of $8.25\,\mathrm{A}$, which is two orders of magnitude smaller than what modern gradient amplifiers achieve, the image quality is not perfect, but surprisingly good. The image quality could be improved significantly with an industrially manufactured high-performance gradient coil integrated into a comparable Bruker system [120]. One 256×256 image is shown in Fig. 3.16b.

3.3.3 Human System

After the initial PatLoc measurements on the Bruker hardware, a second PatLoc coil was developed and integrated into a MAGNETOM Trio, A Tim System $3\,\mathrm{T}$ (Siemens Healthcare, Erlangen, Germany). The goal was to

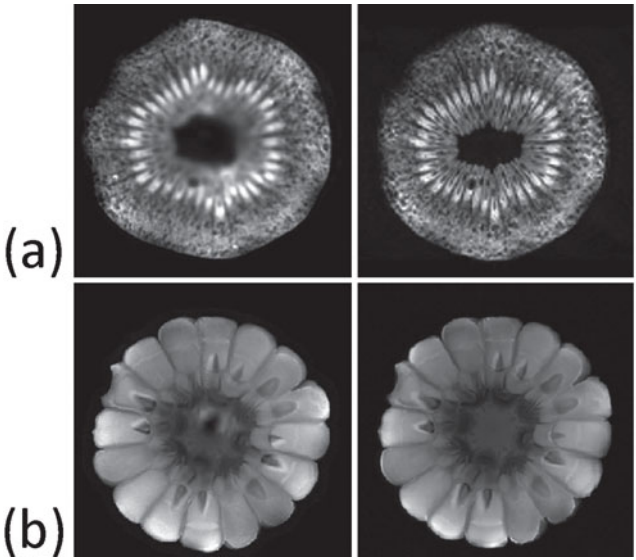

Figure 3.16: Measurement results with the small-bore system. (a) On the left, one of the very first reconstructed images is shown acquired with the PatLoc prototype coil. Shown is the image of a kiwi fruit. On the right, a reference image is shown acquired with the standard gradient system. The same imaging parameters were chosen. (b) With the second-generation small-bore PatLoc coil, the image quality could be improved significantly. Shown is a cross-section of a corn cob acquired with a spin echo sequence. On the left, the PatLoc image, and on the right, a reference image. The images in (b) were produced by Stéphanie Ohrel at Bruker BioSpin MRI GmbH, Ettlingen, Germany, and presented at the Annual Meeting of the ISMRM 2010 in Stockholm. The presentation was directly related to the abstract [120].

perform in vivo imaging of the human head with a PatLoc gradient coil having a reasonable performance.

The intended design was first described in [198]. Coil design and coil characteristics are described in [196, 197] and some information about coil integration into the scanner hardware is given in [[42]]. The safety considerations, evaluated in [[24]], formed the basis for obtaining formal ethics approval for research measurements on human volunteers by the institutional review board of the University of Freiburg. Written consent was obtained from each volunteer prior to all in vivo measurements performed for this thesis.

Figure 3.17: Construction of the PatLoc human head insert coil. From left to right, top row: The new coil consisted of several identical wire elements, which differentiated significantly from the elements of the PatLoc prototype coil. These elements were mounted on a cylindrical former, water cooling was added and the components were fixed with epoxy resin. Bottom row: With the RF coils inside, the coil was then introduced into the scanner bore.

The basic construction steps of the PatLoc coil are depicted in Fig. 3.17 and described in the figure caption. Although the shape of the SEMs, which could be generated with the new coil, was very similar to the fields of the initial PatLoc prototype coil, the approach to achieve this was different. The first PatLoc coil was equipped with a single layer of eight elements. With this design, all eight elements had to be used to generate both quadrupolar SEMs (cf. Fig. 3.14). The new design consisted of two layers, each with four elements. This is depicted in Fig. 3.18a, b. Each layer directly represented one of the quadrupolar SEMs. Fig. 3.19 shows that the generated fields were very similar to exact quadrupolar encoding fields. Note that not only the arrangement of the coil elements, but also the single elements were redesigned. More on the optimization of the design of the elements and the coil itself can be found in [196, 76], [[105]].

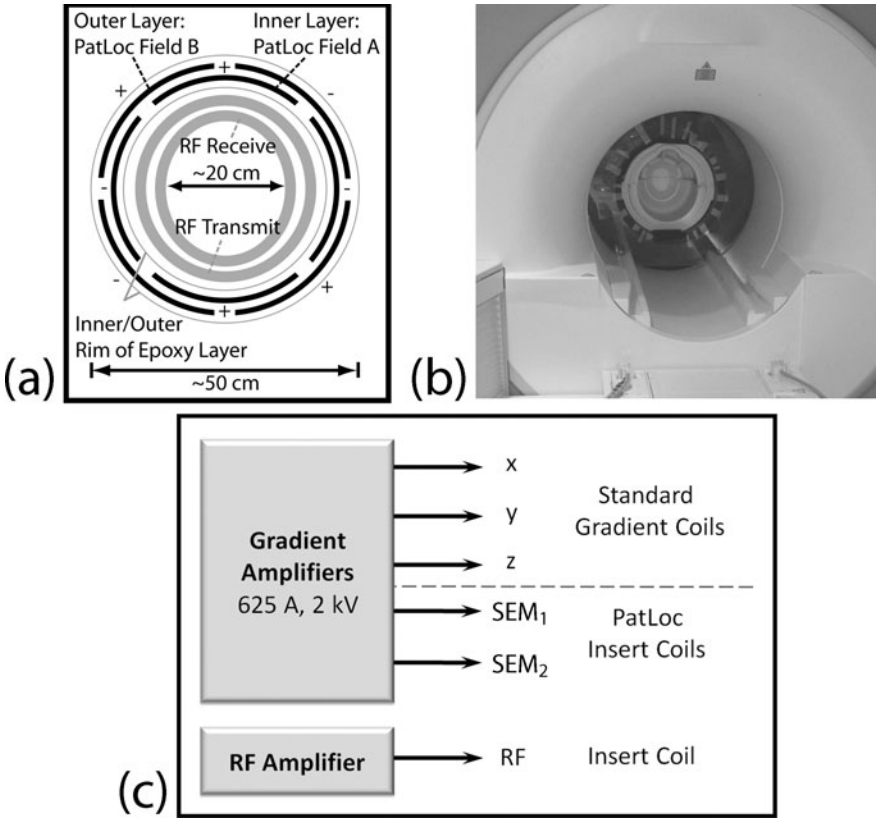

Figure 3.18: The PatLoc human head insert and its integration into the scanner environment. (a) Design of the PatLoc insert. The two-layer structure, with one layer for each SEM, was constructed to generate two orthogonal quadrupolar SEMs by alternating the current directions between adjacent elements. Placed inside, RF-transmit and receiver coils were sized to provide enough space for a human head. (b) The main components of the insert are visible in this photograph. (c) The standard gradient system was complemented with additional channels for independent operation of the gradient coils and the PatLoc head insert.

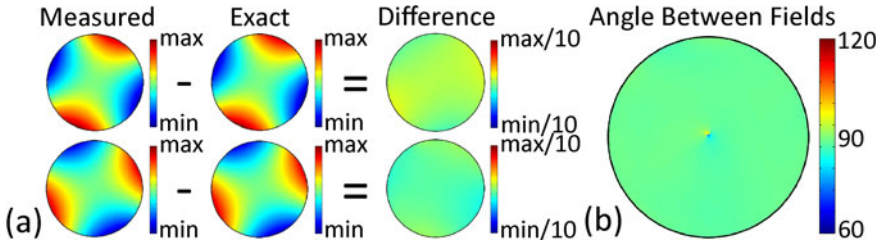

Figure 3.19: PatLoc SEMs generated by the human head insert. (a) Deviation from an exact quadrupolar field geometry. (b) Angle between the two encoding directions. The scaling is the same as used for the prototype small-bore insert coil (cf. Fig. 3.15). Compared to the SEMs of the prototype coil, the SEMs of the human head insert resemble their exact counterparts even more. Deviations are below $2\,\%$ and the encoding directions are almost everywhere close to $90\,^{\circ}$ indicating very high encoding efficiency.

In contrast to the first PatLoc prototype coil, the standard functionality of the scanner was not restricted during PatLoc measurements. The hardware was modified such that the quadrupolar SEMs could be controlled simultaneously and independently from the standard gradient system. The new coil integration approach enhanced the flexibility of the system because more channels were available (with the quadrupolar PatLoc coil, 5 instead of 3) for signal encoding (also cf. Fig. 3.18c).

The most important coil parameters for the small-bore PatLoc prototype coil and the large human head insert are compared with each other in Table 3.1. The comparison of the two coils reveals significant differences. Most obvious, the human head insert is much larger than the prototype insert coil. This explains the better performance of the small-bore prototype coil in terms of resistance, inductance and rise time. More important, however, is that larger objects (like the head) could be measured with the human head insert. Larger objects provide more signal with positive consequences for SNR. Despite the much higher field sensitivity of the small-bore prototype coil, the maximum gradient strength and especially the maximum magnetic field strength achievable with the human head insert is higher; these properties of the head insert are beneficial for image quality, but are still not optimal because the design of the coils allowed only a maximum current of $80\,\mathrm{A}$, much less than the amplifiers could have provided ($625\,\mathrm{A}$). Problematic with the measurements on the small-bore system was that the PatLoc prototype coil could only be driven with a low current of $8.25\,\mathrm{A}$. Therefore,

Table 3.1: Comparison of important coil parameters of the first small-bore prototype insert and the human head insert.

Parameter	Insert: Small-Bore	Human Head
usable diameter (with RF inside) [cm]	6	20
usable length [cm]	6	> 20
maximum current [A]	8.25	80
inductance [μH]	30	2200
resistance [mΩ]	400	510
rise time [μs]	24	200
dwell time [μs]	100	10
field sensitivity[8] [$\mathrm{mT/Am^2}$]	26.1	1.44/1.36
max. gradient at the periphery [$\mathrm{mT/m}$]	12.9	22.5
max. field strength at the periphery [mT]	0.2	1.1

the dwell time had to be chosen fairly large, setting a considerable lower bound on the choice of the echo time. Also, the large dwell times and SNR restrictions hindered the acquisition of high-resolution images with the first small-bore prototype coil.

The overall assessment of these parameters reveals that measurements with the human head insert should be more flexible and a higher image quality is to be expected. Measurements performed with the human insert confirm this assessment. As an example, an image of a fruit basket, which has been acquired with the head insert, is compared in Fig. 3.20 to the PatLoc prototype kiwi image shown in Fig. 3.16a.

Once the system had been set up correctly, it was not problematic to acquire high-resolution images with the human head insert. The image of the fruit basket has no geometric distortions; only some residual aliasing artifacts are visible, which are related to inaccuracies in the determination of the RF-sensitivity profiles. These artifacts are tolerable because they appear only at the low-resolution center.

[8] Field sensitivity of the outer and inner layer (cf. Fig. 3.18). With a different method, $1.42\,\mathrm{mT/Am^2}$ was measured for the inner layer and $1.30\,\mathrm{mT/Am^2}$ for the outer layer.

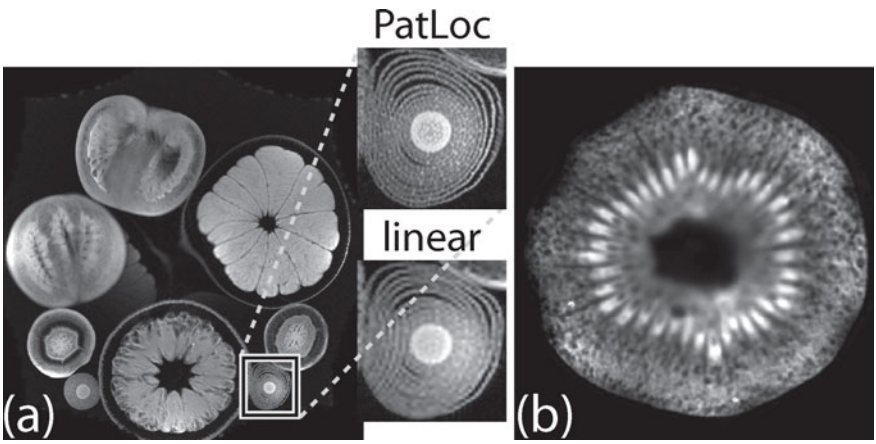

Figure 3.20: Comparison of PatLoc images acquired with the human head insert (a) and with the older small-bore prototype coil (b). The fruit basket was reconstructed from 384^2 data points. In compliance with the specifications of the prototype coil, only 128^2 data points were acquired for the kiwi fruit. The comparison of the zoomed-in sections of the PatLoc acquisition and an identical measurement, but encoded with the standard gradient system, shows that the image quality could be enhanced significantly compared to the first prototype system.

The problems associated with the first small-bore prototype coil could be solved with the second-generation small-bore PatLoc coil [120] and an image quality was achieved that is in no way inferior to the images found with the human head insert (cf. Fig. 3.16b). Currently, a high-performance coil is being manufactured also for the human system. The new coil will allow detailed assessment of image quality and fair comparison with conventional state-of-the-art gradient systems integrated into human systems.

Contributions of this Thesis and Current State of Research

THIS is a brief overview. More details about the major findings of this thesis are found in the summary, chapter 8.1, page 277ff, and important literature is presented where it seems most appropriate.

Contributions of This Thesis Before this thesis was conducted conceptual ideas about PatLoc imaging had existed, and initial numerical simulations had substantiated the feasibility of MRI with NB-SEMs if combined with parallel image acquisition techniques [62]. A simplified encoding model had been used with non-overlapping RF-coil sensitivities that allowed straightforward image reconstruction. PatLoc measurement hardware had not yet been designed.

The main goal of this thesis was to elaborate the theoretical basis of PatLoc signal encoding, to develop efficient image reconstruction methods, and to evaluate these with numerical as well as experimental data, including in vivo measurements. In chapter 4 common principles of PatLoc encoding and reconstruction are presented. In chapters 5 to 7, reconstruction algorithms and imaging results are analyzed in detail for several PatLoc encoding strategies. The subsequent chapters therefore reflect the scientific outcome that is in line with the main focus of this thesis; also, the two primary own publications [[156, 158]] concern this part of the thesis.

A significant part of the scientific output also concerns other topics; among others, hardware, methods, applications. However, the main responsibility for these topics rested with other members of the PatLoc team; the PatLoc overview in chapter 3 is presented with a focus on topics that have resulted in (co-)authorship[1] contributions, for example [[61, 156, 42, 207, 63, 199, 24]].

Also the introductory chapter 2 contains material of scientific value. Its main impact lies on the conceptual level; some of the most important state-of-the-art MR image reconstruction methods are related to a common principle,

[1] It is repeated here that double brackets, [[·]], indicate own (co-)authorship.

thereby establishing interesting connections between them - as well as between existing methods and PatLoc image reconstruction, as shown in chapter 4. Moreover, in chapter 2.3.1e the superresolution effect of RF encoding is quantified. Further contributions are found in the appendix, sections A.3 to A.5.

A full list of own publications is included below on page 329ff.

Current State of Research Prior to the PatLoc project, benefits from using NB-SEMs had rarely been discussed in the literature; among the few publications are [193, 110, 208, 131, 128, 126]. Each of these publications presents very interesting ideas; however, only specific aspects with very special field geometries are discussed therein. No attempt had been undertaken to develop a general imaging concept - like PatLoc imaging. These publications have had an impact on this thesis in some places; the major influence, however, comes from literature that deals with standard parallel image acquisition, most notably [173, 135, 134, 49].

In the meantime, several research groups have contributed important ideas to the growing field of imaging with NB-SEMs. Especially the group of Todd Constable (for example [22, 178, 41, 181]) from Yale university, USA, has to be mentioned, and Fa-Hsuan Lin (for example [97], [[101]]) from the Massachusetts General Hospital, USA. Recently, Layton et al. [93] from the university of Melbourne, Australia, have published interesting research results; actively involved is the research group of Rudolf Stollberger from the University of Graz, Austria, [[86]]. Noteworthy is also [87] by Kopanoglu et al. from Bilkent University, Ankara, Turkey, and the excellent work of Peter Jakob's group from the University of Würzburg, Germany, [203, 1].